Quaternary Science Advances 13 (2024) 100145

Contents lists available at ScienceDirect

Quaternary Science Advances

journal homepage: www.sciencedirect.com/journal/quaternary-science-advances

The contemporary stable isotope hydrology of Lake Suigetsu and surrounding catchment (Japan) and its implications for sediment-derived palaeoclimate records

Charlie L. Rex [a,*], Jonathan J. Tyler [b], Kazuyoshi Nagaya [c], Richard A. Staff [a], Melanie J. Leng [d], Keitaro Yamada [e], Ikuko Kitaba [e], Junko Kitagawa [c], Hideaki Kojima [f], Takeshi Nakagawa [e]

[a] Scottish Universities Environmental Research Centre (SUERC), University of Glasgow, Scottish Enterprise Technology Park, Rankine Avenue, East Kilbride, G75 0QF, UK
[b] Department of Earth Sciences, University of Adelaide, Adelaide, South Australia, 5000, Australia
[c] Varve Museum, 122-12-1 Torihama, Wakasa-cho, Mikatakaminaka-gun, Fukui Prefecture, 919-1331, Japan
[d] National Environmental Isotope Facility, British Geological Survey, Keyworth, NG12 5GG, UK
[e] Research Centre for Palaeoclimatology, Ritsumeikan University, 1-1-1 Noji-higashi, Kusatsu, Shiga Prefecture, 525-8577, Japan
[f] Wakasa Mikata Jomon Museum, 122-12-1 Torihama, Wakasa-cho, Mikatakaminaka-gun, Fukui Prefecture, 919-1331, Japan

ARTICLE INFO

Keywords:
Stable isotopes
Precipitation isotopes
Lake water isotopes
East Asian monsoon
Sediment cores

ABSTRACT

The Lake Suigetsu sediment cores exemplify a high-quality archive of palaeoclimatic change in East Asia during the past 150 ka. Robust interpretation of stable isotope-based proxy reconstructions from the Suigetsu cores can be aided by a greater understanding of the factors affecting the isotope composition of the lake and how it relates to that of precipitation. Here we use extended contemporary monitoring to establish the factors affecting the stable isotope composition ($\delta^{18}O$, $\delta^{2}H$ and d-excess) of precipitation, river water and lake water in the catchment surrounding Lake Suigetsu, central Japan. We show that the composition of precipitation is influenced by the dual East Asian Monsoon system, producing minima in $\delta^{18}O$ and $\delta^{2}H$ and semi-annually varying d-excess values across the year. These signals are then transferred to the lake system, where they are combined with secondary local influences on lake water composition: homogenisation with existing catchment waters, a catchment transit lag, the interaction with saline water from the nearby Sea of Japan, and evaporative enrichment during summer. Our observations suggest that the palaeo-isotope composition of Lake Suigetsu was closely related to the behaviour of the East Asian Monsoon. We highlight lake stratification and proxy seasonality as critical components of signal interpretation.

1. Introduction

The Five Lakes of Mikata are a collection of tectonic lakes located in Fukui Prefecture, central Japan, and comprise Lake Mikata, Lake Suigetsu, Lake Suga, Lake Kugushi and Lake Hiruga (Fig. 1). To-date, much of the Quaternary research undertaken on the lakes has focussed on Lake Suigetsu, the central lake of the system, by virtue of its unique underlying sedimentary sequence. This sequence is exceptionally well-preserved by a deep water column (34 m) and surrounding hills, which hinder wind turbation; bottom water anoxia, which prevents bioturbation; and a shallow connection (the Seto Channel) between Lake Suigetsu and Lake Mikata (upstream of Lake Suigetsu, Fig. 1C), which prevents disturbances by high energy events (Nakagawa et al., 2021). A series of previous deep coring campaigns have extracted sediment from Lake Suigetsu to generate a high-quality archive of environmental change ("the Lake Suigetsu sediment cores") spanning >98 m from the present day to in excess of 150 ka BP (Nakagawa et al., 2012). A distinctive characteristic of the Suigetsu cores is that they contain annual laminations (varves) between ~50 and 10 ka BP, comprising the longest continuously varved record from the Quaternary (Schlolaut et al., 2012). The youngest sediments (up to 50.3 ka BP) have been dated to high precision using radiocarbon dating of >800 macrofossils (Staff et al., 2011; Bronk Ramsey et al., 2012, 2020), varve counting using optical microscopy (Schlolaut et al., 2012, 2018), and analysis of volcanic tephra deposits with independent ages (e.g., Smith et al., 2011; McLean et al., 2016). Between 50.3 ka BP and 13.9 ka BP, Lake Suigetsu

* Corresponding author.
E-mail address: c.rex.1@research.gla.ac.uk (C.L. Rex).

https://doi.org/10.1016/j.qsa.2023.100145
Received 5 October 2023; Received in revised form 3 November 2023; Accepted 6 November 2023
Available online 19 November 2023

contributes the only non-reservoir corrected dataset within the international consensus radiocarbon calibration curve, "IntCal".

It is this excellent archive preservation and world-leading chronological control which makes multiproxy palaeoenvironmental analyses of the Suigetsu cores an exciting prospect. Indeed, the location of Lake Suigetsu at a lower latitude than other global benchmark records (e.g., the Greenland and Antarctic Ice Cores) makes this archive an avenue for establishing a more holistic global perspective on past climatic change. Additionally, the Japanese archipelago is situated within the East Asian Monsoon (EAM) regime, a critical, yet complex, component of the global climate system for which palaeoclimate reconstructions offer a means to greater understanding. Not only is Japan situated directly beneath the seasonally migrating EAM front, making it sensitive to changes in the EAM system (Jun-Mei et al., 2013; Nakagawa et al., 2012; Gallagher et al., 2018), but unlike continental areas, Japan experiences EAM precipitation semi-annually (twice a year), because both the winter (EAWM) and summer (EASM) prevailing monsoon winds pass over large bodies of water before reaching the Japanese Islands. Therefore, both seasonal modes have tangible hydrological influence over precipitation in Japan, and reconstructions from here have the unique potential to

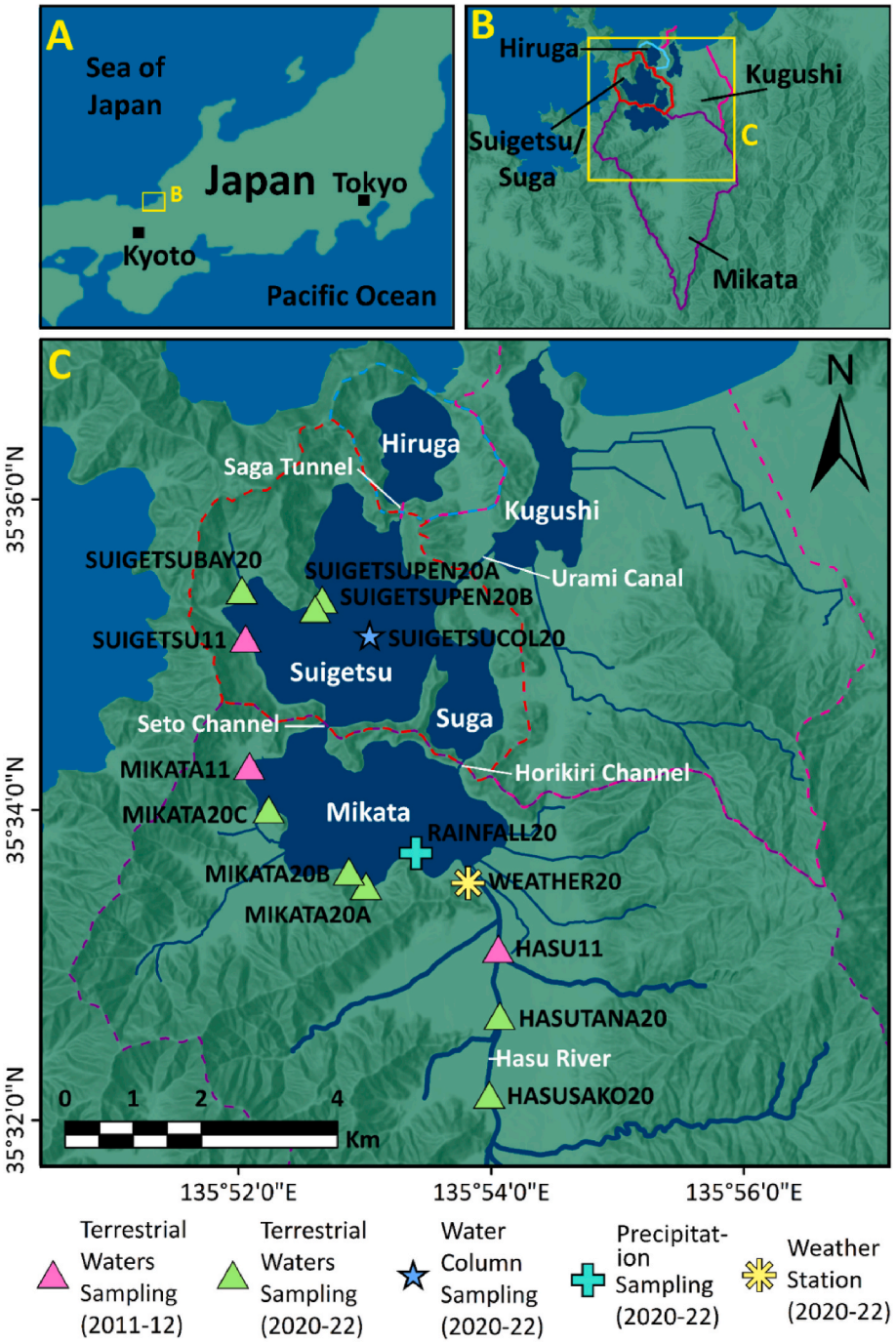

Fig. 1. Map of the Five Lakes of Mikata catchment. Yellow outlines show the extent of subsequent panels in the sequence. Panel A shows the location of the region in relation to major Japanese cities. Panel B shows the catchment area of each lake. Panel C shows the sampling locations for this study, including precipitation sampling, river and lake sampling, and sampling of the Lake Suigetsu water column, as well as the location of the weather station. Full details of locations shown here are available in Appendix A. Basemaps: custom World Dark Grey Base and World Hillshade from Esri (2022a, 2022b) (scale 1:10,000,000 (Panel A), 1:400,000 (Panel B), 1:67,946 (Panel C)). (For interpretation of the references to colour in this figure legend, the reader is referred to the Web version of this article.)

determine the behaviours of both the EAWM and the EASM. In light of this, the Suigetsu cores continue to be the subject of an ever-growing collection of investigations into climatic change over the last glacial-interglacial cycle (e.g., Schlolaut et al., 2017; Nakagawa et al., 2021), including contributing to the definition of the Holocene onset as an auxiliary stratotype (Walker et al., 2009). An ongoing avenue of research is the development of palaeoclimate reconstructions derived from oxygen and hydrogen isotope compositions of pollen grains, biogenic silica and siderite (all of which are abundant components of the cores), because these offer a means to infer past hydrological change (including links to EAM behaviour).

Robust interpretation of such sedimentary proxies is predicated on a strong understanding of the controls acting on lake isotope composition (δ_{lake}), which, in the absence of historical datasets, can be achieved by extended contemporary monitoring. Of particular interest is the extent to which variability in the isotope composition of precipitation ($\delta_{precipitation,}$ which provides a link to regional-scale hydrological change) is reflected in the isotope composition of river water (δ_{river}) and δ_{lake} and, in turn, lake sedimentary components; however, this depends strongly on catchment and lake hydrology. Variability in groundwater, river, and in rare cases, marine contributions to the lake water balance can act to dampen and sometimes conceal the isotope composition of recent precipitation (e.g., Seal and Shanks, 1998; Lacey and Jones, 2018). In addition, evaporation of lake waters can strongly modify δ_{lake} compared to inflowing water (Gonfiantini, 1986; Russell and Johnson, 2006; Wassenaar et al., 2011). These concepts are commonly used in modern hydrology (Gibson et al., 2016); for example, during mass balance modelling to determine the surface versus groundwater contribution to Lake Ohrid, south-eastern Europe (Lacey and Jones, 2018) or to consider mass losses due to evaporation, such as for Lake Edward, East Africa (Russell and Johnson, 2006). Monitoring for an extended period (on the order of years) is required in order to fully understand the evolution of δ_{lake}, particularly in regions where the climate is so seasonal. This approach allows for both local influences (such as changing inputs and evaporation) to be identified alongside regional scale climatic shifts.

In this study we aimed to better understand the controls acting on the isotope composition of water within Lake Suigetsu and its surrounding catchment, in order to facilitate interpretation of isotope-based proxy reconstructions of past climate from the Lake Suigetsu sediment cores. By monitoring $\delta_{precipitation}$, δ_{river} and δ_{lake} over a total observation period of two years and ten months across 2011–2012 and 2020–2022, we assessed the factors affecting the relationships between these variables. Conceptualising δ_{lake} of Lake Suigetsu is particularly important because whilst the lake and catchment receive high volumes of precipitation annually, there are other controls which could act to alter or obscure this precipitation signal; namely, that expected evaporation rates are high due to a warm summer climate, and in the present day there is some interaction between the lake and the Sea of Japan. Consequently, resolving the relative influence of $\delta_{precipitation}$ (and the propagation of $\delta_{precipitation}$ signals to δ_{lake}) is crucial to understanding the major controls over long term δ_{lake} within the context of regional scale hydrological (and thus climatic) change.

2. Study site

2.1. Hydrology

The Five Lakes of Mikata are located adjacent to the towns of Wakasa and Mihama in Fukui Prefecture, Honshu Island, central Japan. The lakes lie to the west of the active Mikata fault line and were formed as the western side of the fault subsided over time (Fig. 1C; Nakagawa et al., 2012). Over the last ~400 years, the Five Lakes of Mikata catchment has been anthropogenically influenced by the construction of channels and tunnels to connect the lakes. In the present day, the lakes form a route between the freshwater Hasu River and the saline Sea of Japan (Fig. 1C). Lake Mikata, the southernmost lake, is fed by the Hasu River to the south, has an area of ~3.61 km^2 and a maximum depth of 5.8 m and has the largest discrete catchment area (~50 km^2; Fig. 1B). Lake Mikata is connected to Lake Suigetsu via the shallow (~2 m deep) Seto Channel, and to the adjacent Lake Suga via the artificial (<0.5 m deep) Horikiri Channel. Lake Suigetsu, which has an area of ~4.2 km^2 and a maximum depth of 34.0 m, then feeds Lake Hiruga (via the subterranean Saga Tunnel, which was sealed during the observation period) and Lake Kugushi (via the surficial Urami Canal), which both flow directly into the Sea of Japan (Shigematsu et al., 1961, Fig. 1C). In the past, prior to the construction of the Horikiri Channel, Saga Tunnel and Urami Canal, Lake Kugushi was a coastal lagoon (part of Wakasa Bay), and Lake Hiruga was not connected to the sea (except during flooding), so four of the five lakes were freshwater (Shigematsu et al., 1961; Masuzawa and Kitano, 1982). At this time, the outflow from Lake Suigetsu was via Lake Suga (effectively a side basin of Lake Suigetsu), which was connected to Lake Kugushi via a channel (the Kiyama River) through low ground to the east of the lakes.

Principally, water flows in a south-to-north direction through the catchment, driven by the large quantities of precipitation in the region. However, in the present-day, seawater washes back into Lake Suga, Lake Suigetsu and Lake Mikata during high tide in autumn (Kondo and Butani, 2007). As a result, all five lakes now have some degree of marine-derived salinity and observations show that salinity in the lakes increases during the autumnal high tide and then decreases due to continued freshwater input via precipitation and surface runoff during winter. Lake Hiruga and Lake Kugushi are saline, and Lake Mikata is fresh to brackish (0–3 g kg^{-1}). Lake Suigetsu and Lake Suga are both meromictic (permanently stratified), with an upper mixolimnion (aerobic, brackish to saline water; 2–8 g kg^{-1}) separated from a lower monimolimnion (anaerobic, saline water; ~13 g kg^{-1}) by a chemocline at ~8 m depth (Matsuyama, 1974; Kondo et al., 2000; Kondo and Butani, 2007). The mixolimnion exhibits a salinity gradient between the surface (fresh) and the chemocline (saline) (Matsuyama, 1974; Kondo et al., 2000). Mixing in the mixolimnion occurs once each year, during the autumn, resulting in an increase in surface water salinity, a raised chemocline and a steepening of the salinity gradient (Kondo et al., 2000). The chemocline then lowers and a shallower salinity gradient is re-established during winter. The monimolimnion is a persistent seawater-derived saline layer, confirmed by geochemical analysis (Shigematsu et al., 1961), and has a limited freshwater influence (Matsuyama, 1973). This layer is replenished annually at the autumnal high tide (Kondo and Butani, 2007). It is not known whether this autumn seawater incursion drives mixing in the upper ~8 m of the water column, or if these two processes are merely coincident, although the latter is suspected. No significant long-term increases in salinity have been observed in the monimolimnion in the past 70 years; salinity remained approximately 12–16 g kg^{-1} in the intervals 1951–1966 and 2008–10 (Matsuyama, 1973; Kondo et al., 2014). Complete lake water vertical mixing events are unusual but have been detected (in 1997; Kondo et al., 2000).

The residence time of Lake Suigetsu was calculated to be on the order of ~1 year, assuming a total annual precipitation of ~2.3 m (Japan Meteorological Agency, 2022) across a ~60 km^2 catchment (~0.14 km^3 precipitation annually) and then applying this to a simple single box model (surface area of ~4.3 km^2 and ~34 m depth equating to a ~0.15 km^3 volume). However, when considering the evidence for a stable monimolimnion in Lake Suigetsu with a very long residence time (Shigematsu et al., 1961), a two-box model is more appropriate, with water effectively flushing solely through the top ~8 m of the lake (Matsuyama, 1973). In this case, the residence time of the mixolimnion is on the order of ~3 months.

2.2. Climate

The climate of the Five Lakes of Mikata catchment is temperate with

high levels of precipitation. The temperature profile is typical of Japan, with low temperatures in winter (reaching a minimum in January with a mean temperature of 4.3 °C) and high in summer (reaching a maximum in August with a mean temperature of 27.0 °C). The annual distribution of precipitation is more unusual, because a large proportion of the total annual precipitation falls during winter (Fig. 2). This is unlike much of Japan, where summer is the wettest season. The large quantities of precipitation received in winter are a result of the catchment being located on the Sea of Japan coast, where it receives a significant input of EAWM precipitation annually. This EAWM precipitation falls as both rain and snow and is concentrated in December and January. Spring (March to May) is the driest season of the year, which precedes a second rainy period in early summer which accompanies the EASM. The EASM rainy season is known as the *Tsuyu* or *Baiu,* which occurs at Lake Suigetsu around late June into July, immediately prior to the period of maximum temperature. This is followed by typhoon season from August to September, during which a series of low-pressure systems pass over Japan from the Pacific Ocean to the south, resulting in a third annual period of rain. Winter (EAWM) and summer (EASM) precipitation are the most significant extended (persistent) freshwater inputs to the catchment; typhoon season precipitation comprises a series of intense isolated precipitation events.

3. Materials and methods

3.1. Sampling methods

Samples of lake and river waters (n = 463) were taken from the Hasu River, Lake Mikata and Lake Suigetsu (Fig. 1C) on a weekly basis between 1st March 2011 and 3rd January 2012, and again between 15th July 2020 and 29th July 2022. Water was collected by submerging a collection vessel in the top ~50 cm of water before subsampling using a vial leaving no or minimal head space. Precise sampling locations were altered between the 2011/12 and 2020/22 sampling intervals, and during periods of inaccessibility (e.g., due to bridge repairs, snowfall, lake freezing and flooding; Appendix A). The slight changes in sampling location are unlikely to affect the isotope composition recorded, being within the same water depth range and situated away from lake inputs. If visible algae were present in the water, the samples were filtered using a 50 μm polyethylene terephthalate (PET) mesh filter. Surface water data from the 2011–2012 observation period do not have the accompanying (precipitation and water column) data described below in Section 4 because this was an extended pilot study focussed on the river and lake waters; however, we have nevertheless included these 2011–2012 data in our analysis because there are subtle differences in these data that contribute to a more comprehensive view of isotope variations in the catchment.

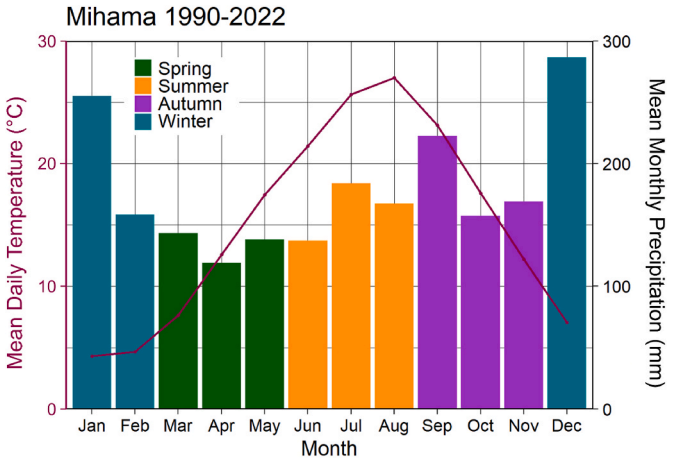

Fig. 2. Climate at the Five Lakes of Mikata. Monthly variations in mean daily temperature (pink curve) and mean total monthly precipitation (bars) at Mihama, adjacent to Lake Kugushi (35°36′00″N 135°55′00″E). Data from the Japan Meteorological Agency, 1st January 1990 to 28th February 2022. (For interpretation of the references to colour in this figure legend, the reader is referred to the Web version of this article.)

Precipitation samples (n = 120) were captured between 13th July 2020 and 29th July 2022 using a purpose built (3D printed) funnel and glass bottle holder in Wakasa (at the location indicated in Fig. 1C). Silicone oil was added to the collection bottle to prevent evaporation. Water subsamples were taken from the bottle using a Teflon pipette. Subsamples were taken on an event basis; every day during periods of frequent precipitation, but less often during periods of reduced precipitation. The water was allowed to overflow the sample vial in order to remove the floating silicone oil. Fresh snowfall samples were collected from pristine areas of snow after deposition and melted with silicone oil in a lidded container before being transferred to the collection vial. An automated Netatmo weather station (location also shown in Fig. 1C) was deployed to provide temperature, humidity, precipitation amount and wind data to accompany the isotope data. Backwards air parcel trajectory analysis was performed for four precipitation events (representative of each season) using the NOAA Air Resources Laboratory HYSPLIT model (Stein et al., 2015; Rolph et al., 2017). The selected events ended on 27th December 2020, 16th September 2021, 2nd May 2022 and 7th July 2022, respectively. Back trajectories were generated for air parcels arriving at the catchment every 12 h at 1500 m.a.s.l. across a 72-h window prior to the end of each event.

Water column profiling was conducted ~quarterly on 22nd December 2020, 8th April 2021, 5th August 2021, 17th November 2021, 23rd April 2022 and 21st July 2022 at the approximate centre of Lake Suigetsu (Fig. 1C). Samples were taken every 2 m between the surface and 10 m depth, every 5 m between 10 m and 30 m depth, and then every 2 m between 30 m and 34 m (n = 70). A sealable van Dorn water sampler was used to prevent mixing of the sample with water at different depths during transit to the surface. A Hydrolab DS5 water quality meter was also used to measure temperature and salinity profiles on each sampling date; higher resolution geochemical data were collected for the December 2020, April 2021, November 2021, April 2022 and July 2022 dates. The low-resolution data collected for the August 2021 date (using a TOA-DKK WQC-24 m) are also shown in Section 4 below.

3.2. Analytical methods

Oxygen isotope ($\delta^{18}O$) measurements were made using an Isoprime 100 mass spectrometer with an Aquaprep dual-inlet system using the CO_2 equilibration method. Subsamples (totalling 200 μl) were placed in a heated sample tray at 40 °C before the air was evacuated and each exetainer was flushed with CO_2. The samples were then left to equilibrate for between 12 (first sample) and 37 (last sample) hours. Any remaining water vapour was then removed on a sample-by-sample basis using a cryogenic water trap, before each sample was expanded into the dual inlet isotope ratio mass spectrometer (IRMS) for analysis. The samples were measured in alternate pulses alongside a reference CO_2 gas, and the integrated values of the sample were compared to the reference gas values to determine $^{18}O/^{16}O$. Two internal laboratory standards (CA-HI and CA-LO) were analysed in each run. The value of these standards has been determined accurately by comparison with international calibration and reference materials (VSMOW2, SLAP2 and GISP). This facilitated the calculation of the $^{18}O/^{16}O$ ratio of each sample versus VSMOW2, and subsequent expression of the oxygen isotope ratio in delta (δ) units ($\delta^{18}O$) in parts per mille (‰). The typical standard deviation is < 0.05 ‰.

Hydrogen isotope ($\delta^{2}H$) measurements were made in duplicate using a continuous flow, high temperature conversion elemental analyser - IRMS (TC-EA-IRMS) (EuropyrOH-Isoprime) with liquid autosampler. Subsamples (0.5 μl) were injected into a heated septa-sealed port at 160 °C and converted to water vapour. The vapourised sample was then

flushed through a chromium-packed reactor at 980 °C by the helium carrier gas, which reduced the water to hydrogen gas. A reference hydrogen gas pulse was introduced to the IRMS prior to the gas pulse from each sample. The sample peaks were then integrated and corrected for the H_3^+ contribution before comparison to the reference gas to yield $^2H/^1H$. Each sample was measured five times. As with the oxygen isotope measurements, the samples were then compared to measurements of CA-HI and CA-LO to calculate the $^2H/^1H$ ratio of each sample versus VSMOW2, and expression of the hydrogen isotope ratio in delta units as for the oxygen isotopes. The typical standard deviation is < 0.5 ‰.

The aforementioned $\delta^{18}O$ and δ^2H measurements were then used to calculate d-excess (Equation (1)), a second-order parameter which can be considered as a measure of deviation from the Global Meteoric Water Line (GMWL, which has a gradient of 8). This occurs when there is a greater amount of ^2H relative to ^{18}O, caused by diffusive fractionation during evaporation of water molecules (Bershaw, 2018).

$$d - excess = \delta^2H - (8 * \delta^{18}O) \quad \text{(Equation 1)}$$

4. Results and interpretation

4.1. Precipitation $\delta^{18}O$ and δ^2H

Values of $\delta^{18}O$ for the precipitation at Wakasa (July 2020 to July 2022) ranged from −13.2 ‰ to −2.4 ‰, with a mean value of −7.0 ‰ and standard deviation of 1.6 ‰ (Fig. 3A). δ^2H values ranged from −96.4 ‰ to 2.3 ‰, with a mean of −39.1 ‰ and standard deviation of 11.9 ‰. Fig. 3A shows only small seasonal differences in $\delta^{18}O$ and δ^2H because there was considerable intra-seasonal variability and overlap. Throughout the study period, $\delta^{18}O$ and δ^2H were associated with rapid high amplitude fluctuations with time (Fig. 4); however, winter and summer minima were observed when the data were considered on a monthly basis; likely due to greater quantities of precipitation (Fig. 2) during these seasons (discussed in Section 4.4). This trend was clearest in the $\delta^{18}O$ values, but a summer minimum was also observed in the δ^2H values (Fig. 4); the winter minimum likely obscured by high d-excess values (described in Section 4.2). Back trajectory analysis of four precipitation events from across our sampling period indicates that air parcels arriving at the catchment predominately originated over Continental Asia during the winter, in the oceanic domain (Pacific Ocean, Philippine Sea and East China Sea) during summer, and a mixture of the two during the spring and autumn (Fig. 5).

These trajectories, which ultimately reflect the operation of the EAM as dual EAWM and EASM modes, highlight the influence of the EAM on the climate of Japan, and can explain the lack of distinctive seasonal precipitation $\delta^{18}O$ and δ^2H trends at Wakasa. EAWM and EASM precipitation over Japan generally have very similar compositions (Taniguchi et al., 2000; Uemura et al., 2012) in direct contrast to Continental Asia, where EAWM and EASM precipitation exhibit distinct compositions due to continental ($\delta^{18}O_{precipitation} \sim -4$ ‰) versus oceanic sources ($\delta^{18}O_{precipitation} \sim -10$ ‰), and hence vary seasonally (Araguás-Araguás et al., 1998). EAWM air masses originate in central Asia and Siberia and are predominately cold and dry, and hence whilst distillation and moisture recycling earlier in the trajectory is possible, the isotope signal of EAWM precipitation over Japan is dominated by the interaction of this air mass with the Sea of Japan. The evaporation from the Sea of Japan in winter has a light isotope signal ($\delta^{18}O \sim -8$ ‰; Uemura et al., 2012) and the transport distance is short (on the order of <1000 km), so this signal is retained in winter precipitation $\delta^{18}O$ and δ^2H (i.e., little further depletion of the heavier isotopes occurs during transport). Conversely, EASM air masses originate over the Pacific Ocean and track towards the Japanese archipelago via the Philippine Sea and East China Sea (the trajectory ultimately determined by the positioning of the Western Pacific Subtropical High (Xu et al., 2020, Fig. 5). Evaporation from this oceanic domain has a range of isotope compositions (from $\delta^{18}O \sim -4$ ‰ in the Western Pacific Warm Pool to $\delta^{18}O \sim -8$ ‰ in the East China Sea; Uemura et al., 2012); however, the distance from the sources with a heavier isotope signal to Japan is greater, such that overall depletion of the heavier isotopes during transport acts to minimise differences between proximal and distal sources. As such, EASM $\delta^{18}O$ and δ^2H is low, as with the EAWM.

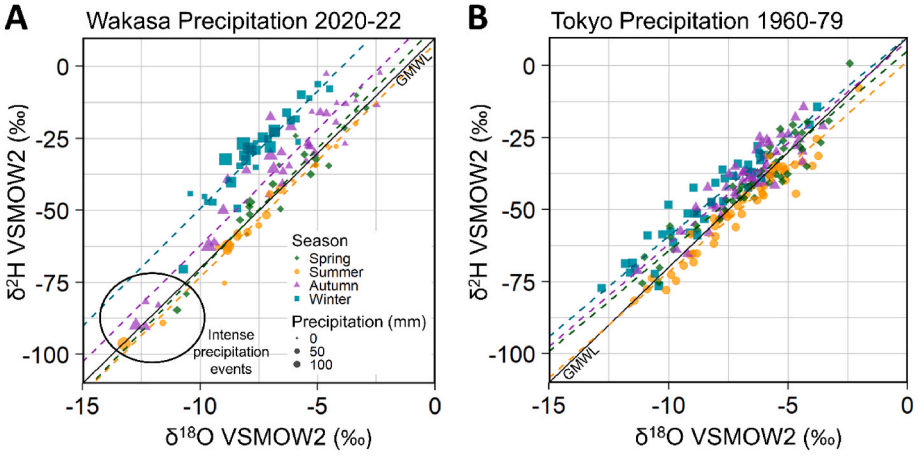

	Wakasa		Tokyo	
	Gradient	Intercept	Gradient	Intercept
Spring	8.5	13.9	7.0	5.1
Summer	7.8	8.1	7.3	1.6
Autumn	8.1	18.5	7.1	8.5
Winter	8.2	32.2	7.2	12.7

Fig. 3. Precipitation $\delta^{18}O$ and δ^2H at Wakasa and Tokyo. A comparison of isotopes in precipitation at (A) Wakasa 2020–22 (event basis, Sea of Japan Coast) and (B) Tokyo 1960–79 (monthly averages, Pacific Ocean Coast). Linear regression local meteoric water lines for each season are shown and numerically described in the table. Black diagonal lines represent the Global Meteoric Water Line (GMWL). The points plotted for the composition of Wakasa are scaled by quantity of precipitation (as calculated from the Wakasa weather station; WEATHER20 in Fig. 1). Seasons are defined as: Spring (Mar–May), Summer (Jun–Aug), Autumn (Sep–Nov), Winter (Dec–Feb). d-excess is higher for points above the GMWL. (For interpretation of the references to colour in this figure legend, the reader is referred to the Web version of this article.)

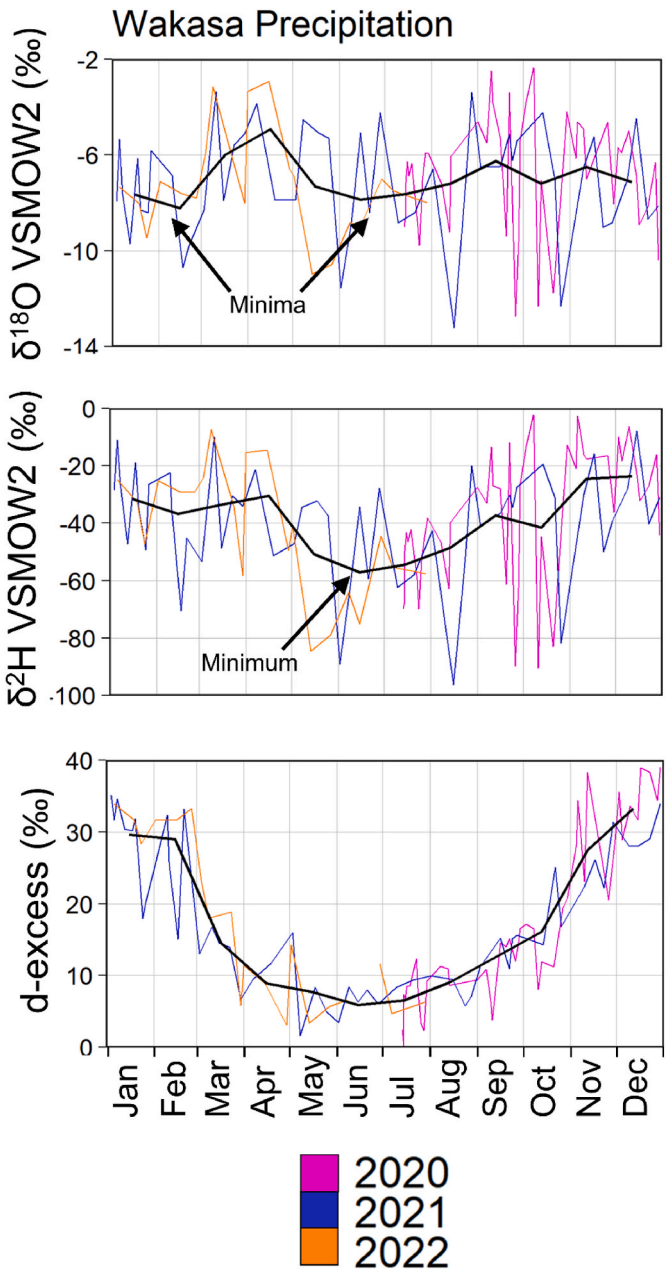

Fig. 4. Variations in $\delta_{precipitation}$ with time. $\delta^{18}O$, $\delta^{2}H$ and d-excess values from precipitation at Wakasa from across the study period (colour lines). Black lines represent monthly averages of each dataset. (For interpretation of the references to colour in this figure legend, the reader is referred to the Web version of this article.)

This similarity in the composition of precipitation from each end member trajectory likely results in the limited seasonality that we observed at Wakasa. The air parcel trajectories during spring and autumn exhibited mixed behaviour, and we suggest that this lack of strong prevailing wind direction and a mixture of vapour sources during these intermediate seasons produced precipitation with a similar composition to the EAM months, although we suspect that the spring and autumn values were slightly higher due to relatively reduced quantities of precipitation during these seasons (discussed in Section 4.4). Intra-seasonal variability was likely due to subtle differences in the airmass trajectories associated with each precipitation event.

Very low $\delta^{18}O$ and $\delta^{2}H$ values (in the $\delta^{18}O$ range of −13.2 ‰ to −11.0 ‰) were uncommon at Wakasa; however, a minor cluster of precipitation events was nevertheless associated with such values (Fig. 3A). The majority of these datapoints represent precipitation from August to October (Fig. 4) and include rains from Tropical Storm Dolphin (2020). Given the seasonality of such events, a simple explanation could be that this precipitation was derived from tropical storms (typhoons), which are associated with $\delta^{18}O$ values up to 6 ‰ lower than other summer precipitation events, driven by strong fractionation processes in heavy cyclonic precipitation (Lawrence and Gedzelman, 1996; Fudeyasu et al., 2008; Li et al., 2010; Jackisch et al., 2022). However, it is worth noting that precipitation from earlier months of the year also occasionally exhibited these values, and other typhoon events did not. Instead, we posit that these compositions were associated more generally with intense precipitation events. Whilst they do not universally correspond to periods with large quantities of precipitation, this does not preclude a relationship with intense precipitation events because our analysis considered only the total amount of precipitation which fell in the collection period, not the intensity. Not all typhoon events result in intense precipitation at Wakasa due to its location, and many typhoons are associated with high wind speeds alone; hence, some were not associated with very low isotope values during the study period.

4.2. Precipitation d-excess

In contrast to the $\delta^{18}O$ and $\delta^{2}H$ datasets, we observed very clear high-amplitude seasonal patterns in precipitation d-excess, which exhibited an average value of 17.1 ‰ and range of 35.6 ‰ across the entire dataset (Fig. 3A). The values for summer precipitation fell broadly along the GMWL, whereas winter precipitation consistently expressed higher d-excess values, offset yet parallel to the GMWL (Fig. 3A). The autumn and spring d-excess values exhibited intermediate values with some overlap with summer and winter, particularly so for the autumn. Regression lines between $\delta^{18}O$ and $\delta^{2}H$ applied to each season had similar gradients (~8), with minor differences due to the relatively limited amount of data across a narrow range. The difference in intercept between the summer and winter regression lines was 24.1 ‰ (equating to a difference in seasonally averaged d-excess of 23.5 ‰).

Collective observations of d-excess at sites across Japan suggest that this variable shows this distinct pattern regardless of location (Uemura et al., 2012; Hasegawa et al., 2014; Ichiyanagi and Tanoue, 2016). High values of d-excess in winter precipitation and low values in summer precipitation can be attributed to contrasting relative humidity values in the precipitation source regions, which overprints the d-excess of the source water itself (Xia et al., 2018; Uemura et al., 2012). Due to cooler sea surface temperatures (and thus low relative humidity) over the Sea of Japan during the winter, we suggest that winter (EAWM) precipitation exhibits higher d-excess values relative to summer (EASM) precipitation, which originates from the oceanic domain during the summer where relative humidity is high (Araguás-Araguás et al., 1998; Kurita et al., 2015). Relative humidity can affect d-excess via multiple mechanisms, but in the low latitudes the dominant control is the amount of raindrop re-evaporation, and in the mid latitudes oceanic evaporation conditions show greater significance (Xia et al., 2022). The gradual transition of influence between these contrasting extremes suggests that there were no abrupt shifts or interfaces between systems at play in this region during spring or autumn and instead, hydrologically, Japan transitioned gradually between the influence of the EAWM and EASM operational modes; supported by the back trajectory analysis (Fig. 5).

4.3. Quantity-weighted composition

The largest precipitation events during our study interval occurred during winter and, to a lesser extent, during the late summer and early autumn (Fig. 3A), which is in line with the long-term climate data from nearby Mihama (Fig. 2). The largest winter events exhibited higher d-excess values, whilst the largest late summer/early autumn events showed low $\delta^{18}O$ and $\delta^{2}H$ values (as discussed above). This has important implications for the introduction of precipitation to the catchment;

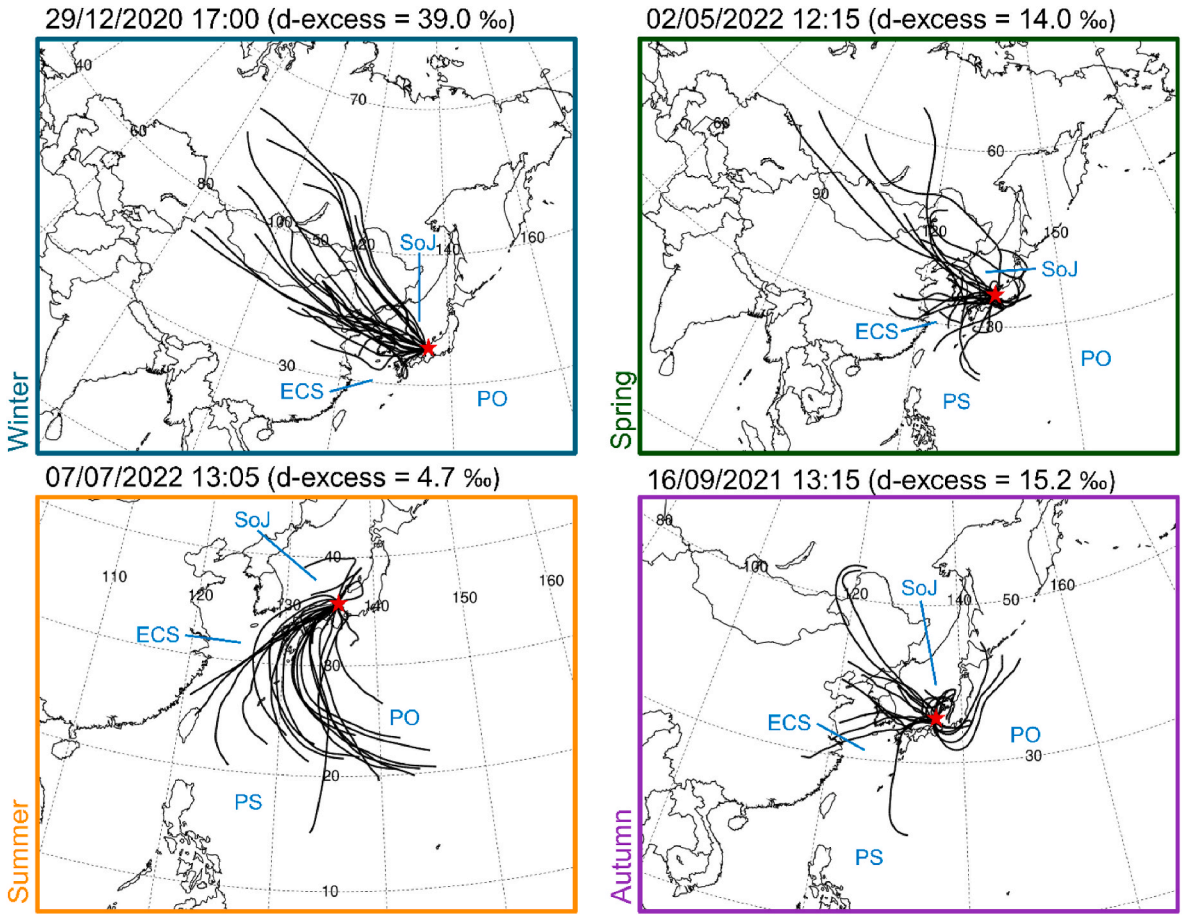

Fig. 5. HYSPLIT back trajectory model results. HYSPLIT back trajectory model results for four rainfall events across the 2020-22 rainfall study period. Events were selected to cover a range of d-excess values which are typical of each of the four seasons. Dates and times indicate the end of each sampling interval. Red stars indicate the position of the catchment; backtrack analysis was performed to the exact position of the precipitation sampler (RAINFALL20 in Figure 1.1). Surrounding seas and oceans are labelled as follows: SoJ = Sea of Japan, ECS = East China Sea, PS = Philippine Sea, PO = Pacific Ocean. (For interpretation of the references to colour in this figure legend, the reader is referred to the Web version of this article.)

most notably, this indicates that the largest contribution to the catchment on an annual basis is that of a mid-range isotope composition (with high d-excess), with a secondary component having low $\delta^{18}O$ and $\delta^{2}H$ values (with low d-excess). When weighted by precipitation amount, the annual mean $\delta^{18}O$ was −7.4 ‰, the annual mean $\delta^{2}H$ was −39.7 ‰ and the annual mean d-excess was 19.8 ‰, which lies between the winter and autumn regression lines. A caveat to this is that the values used to calculate precipitation amount for this analysis were measured by the Netatmo weather station, which did not contain a heating element, so the quantity of precipitation may be underestimated for snowfall events and hence the precipitation-weighted annual mean $\delta^{18}O$ and $\delta^{2}H$ values may lie closer to the winter average. Snowfall events are likely to be amongst the smallest winter precipitation events in Fig. 3A, however, the relatively tight grouping of winter values suggests that the difference between snowfall and rainfall isotope values was not particularly marked across the observation period.

4.4. Temperature and amount effects

Additional analysis (least-squares linear regression) was performed using the precipitation $\delta^{18}O$ and $\delta^{2}H$ values to provide an indication of the influence of a "temperature effect" or precipitation "amount effect". The isotope data were compared to the average temperature and the total precipitation amount (square root transformed) during each collection period, as measured by the Netatmo weather station (position indicated in Fig. 1C). These analyses were conducted using monthly average $\delta^{18}O$ and $\delta^{2}H$ values (to reduce the influence of noise) and then repeated using datapoints from each season in isolation, and the full results are presented in Appendix B. All of the calculated R^2 values were low (0.00–0.34), suggesting that neither temperature nor precipitation amount explained a large proportion of variability in precipitation $\delta^{18}O$ or $\delta^{2}H$. Our findings are in line with other studies, which have suggested that local meteorological parameters are not as prominent as source region and transport effects on precipitation isotopes in Japan (e.g., Hasegawa et al., 2014; Ichiyanagi and Tanoue, 2016); however, others have found that they can retain moderate influence on a local scale (Ichiyanagi and Tanoue, 2016). Our R^2 values are similar to those presented by Ichiyanagi and Tanoue (2016), who found that the $\delta^{18}O$ of precipitation in Fukui City, ~60 km from Lake Suigetsu, showed weak to no correlation with either temperature ($R^2 = 0.02$) or precipitation amount ($R^2 = 0.14$).

Analysing the data by season allows for changes in more dominant influences (e.g., opposing precipitation sources) to be minimised, and thus any obscured temperature and amount effects to be more easily identified. Indeed, this method reveals a stronger relationship between precipitation amount and isotope composition in spring, summer and autumn (but no relationship to temperature during those seasons). This suggests that there was a small amount effect acting on isotopes in precipitation at Wakasa, but no observable temperature effect on event-based timescales. Conversely, winter precipitation isotopes were very weakly correlated with temperature ($R^2(\delta^{18}O) = 0.18$) and not correlated with precipitation amount ($R^2(\delta^{18}O) = 0.00$). However, as

previously mentioned, the Netatmo weather station did not contain a heating element and hence snowfall amount was underestimated. Hence, we posit that there may have been a small amount effect influencing precipitation isotopes during winter, in line with other seasons, but this was not accounted for by our methods. This analysis suggests that the amount effect was a second-order control on isotopes in precipitation at Wakasa but was obscured by seasonality. Indeed, our dataset provides further qualitative evidence for such an amount effect because we observed minima in precipitation $\delta^{18}O$ and $\delta^{2}H$ coinciding with the periods of greatest precipitation amount (excluding the winter $\delta^{2}H$ minimum, observed by high d-excess values) and attributed very low $\delta^{18}O$ and $\delta^{2}H$ values to intense precipitation events. It might be expected that a clearer relationship would be observed between precipitation $\delta^{18}O$ and $\delta^{2}H$ and the integrated amount of precipitation from across the entire transport pathway (as proposed by Uemura et al. (2012)). A lack of any temperature effect was not unexpected, because it has been posited that temperature effects merely explain spatial, not temporal, differences in precipitation isotope composition (Ichiyanagi and Tanoue, 2016).

4.5. Comparison to Tokyo

The isotope composition of precipitation at Wakasa and the nearest GNIP station at Tokyo (350 km to the east) was very similar, albeit with some key disparities (Fig. 3B). The same seasonal patterns in d-excess were observed at both locations, with the summer and winter values acting as end members, and intermediate spring and autumn values. However, compared to Wakasa, the seasonal difference at Tokyo was much less distinct, and the difference between the summer and winter regression line intercept was only 11.1 ‰ (reflecting a difference in seasonally averaged d-excess of 13.0 ‰). This is most likely due to a smaller relative influence of EAWM precipitation (which is associated with the highest d-excess values); Wakasa is located on the Sea of Japan coast, where there is a strong EAWM (and thus Sea of Japan) influence, and Tokyo is located on the Pacific coast, where these influences are significantly weaker. Instead, winter precipitation at Tokyo generally falls in short duration events that result from recycled local water. The local meteoric water line gradients were also shallower and more consistent at Tokyo across the seasons; however, this is likely to be the result of a larger dataset from Tokyo which captured values over a longer timescale. It is important to note that these datasets do not have the same resolution or cover the same period (the Wakasa precipitation dataset is on an event-basis over 2020–22, and the Tokyo precipitation dataset is monthly from 1961-79); however, the same trends are observed when the Wakasa precipitation data is considered at a monthly resolution, and also in comparison to event-based data from Tokyo in 2013 (Appendix C; Ichiyanagi and Tanoue, 2016). Hence, the comparisons made here are reasonable.

4.6. Catchment effects

The seasonal patterns in Hasu River δ_{river} and Lake Mikata and Lake

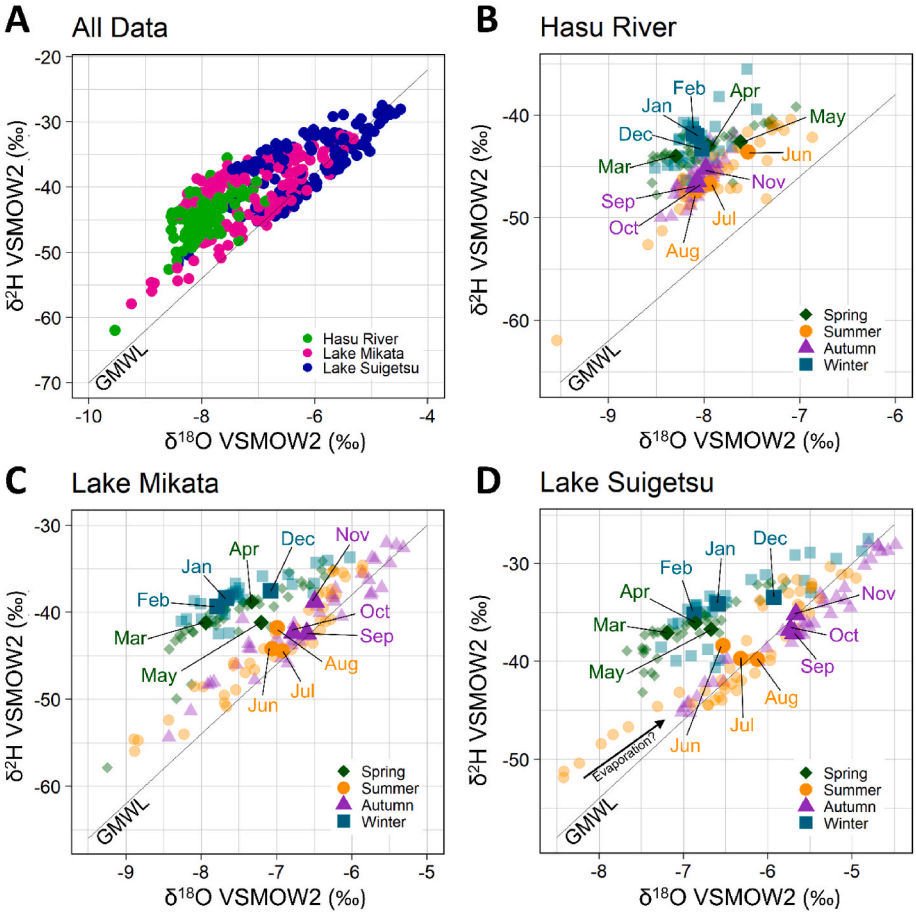

Fig. 6. Surface water $\delta^{18}O$ and $\delta^{2}H$. The isotope composition of surface waters from the Hasu River, Lake Mikata and Lake Suigetsu. Panel A shows differences in composition between parts of the catchment, with colour corresponding to location. Subsequent panels show seasonal variations in composition at (B) the Hasu River, (C) Lake Mikata and (D) Lake Suigetsu. In Panels B–D, monthly averages are shown as opaque symbols and labelled, whilst underlying data points are shown as transparent symbols. Points in Panels B–D are colour-coded by season as in Fig. 3. (For interpretation of the references to colour in this figure legend, the reader is referred to the Web version of this article.)

Suigetsu surface δ_{lake} paralleled those of $\delta_{precipitation}$, showing that the precipitation signals were transferred to the catchment, although there is evidence for some internal modification (Fig. 6). All three locations (the Hasu River, Lake Mikata and Lake Suigetsu) exhibit a smaller range of $\delta^{18}O$ and $\delta^{2}H$ values than precipitation, and hence plot as a tighter grouping of points (range($\delta^{18}O$) = −9.5 to −4.5 ‰, $\sigma(\delta^{18}O)$ = 1.0 ‰ for river and lake water (Fig. 6A) versus −13.0 to −2.5 ‰ and 2.3 ‰ respectively for precipitation (Fig. 3A)), which indicates homogenisation of precipitation inputs with existing catchment waters (likely both surficial water and groundwater). Whilst the isotope composition of groundwater was not quantified as part of this study, and hence remains an unknown input to the lake system, we posit that groundwater composition was merely a slower average of precipitation composition; otherwise, lake water $\delta^{18}O$ and $\delta^{2}H$ would be offset to that of precipitation. We also observed that in-catchment homogenisation attenuated the effect of peripheral values and thus there was a limited influence of isolated events (including the aforementioned intense precipitation events with very low $\delta^{18}O$ and $\delta^{2}H$ values) on the lake system. Instead, prolonged precipitation modes were the more dominant control. Despite annually averaged precipitation being strongly weighted to winter, signals from all four seasons were detectable in the river and lakes (discussed in Section 4.8).

The evolution of $\delta^{18}O$ and $\delta^{2}H$ as water moves through the catchment from the Hasu River to Lake Mikata and then to Lake Suigetsu, also reveals some interesting patterns (Fig. 6A). The Hasu River exhibit a very tight grouping ($\sigma(\delta^{18}O)$ = 0.36 ‰) of low isotope ratios (mean ($\delta^{18}O$) = −7.98 ‰). Isotope values then increased, parallel to the GMWL, as the water moved through to Lake Mikata (mean($\delta^{18}O$) = −7.13 ‰, $\sigma(\delta^{18}O)$ = 0.83 ‰) and then to Lake Suigetsu (mean($\delta^{18}O$) = −6.32 ‰, $\sigma(\delta^{18}O)$ = 0.85 ‰). This suggests some mixing with seawater (which has higher $\delta^{18}O$ and $\delta^{2}H$) in the lakes, with a greater departure in values for Lake Suigetsu, which is the most saline of the three locations (discussed in Section 4.8. Comparatively, the compositions of Lake Mikata and Lake Suigetsu also covered a greater range than the Hasu River. Prior to this study, it was assumed that the Hasu River was the primary input to the lakes, however the differences in the range of their isotope compositions suggests that there was an additional overland (responsive) flow component feeding the lake system and that the river received a substantial groundwater input, producing a more homogenised isotope signal (Fig. 6B). Despite this, the river still reflected the seasonality of precipitation composition, and whilst monthly average composition values for the Hasu River exhibited smaller variations than Lake Mikata and Lake Suigetsu, the signals from the river maintained coincident timing with these parts of the catchment (Fig. 7). These observations suggest that the Hasu River had both direct and groundwater influences on its isotope composition, but we cannot rule out the possibility that weekly sampling of the river did not fully capture the most extreme isotope values here, due to the rate of river flow relative to the sampling resolution and the large catchment area.

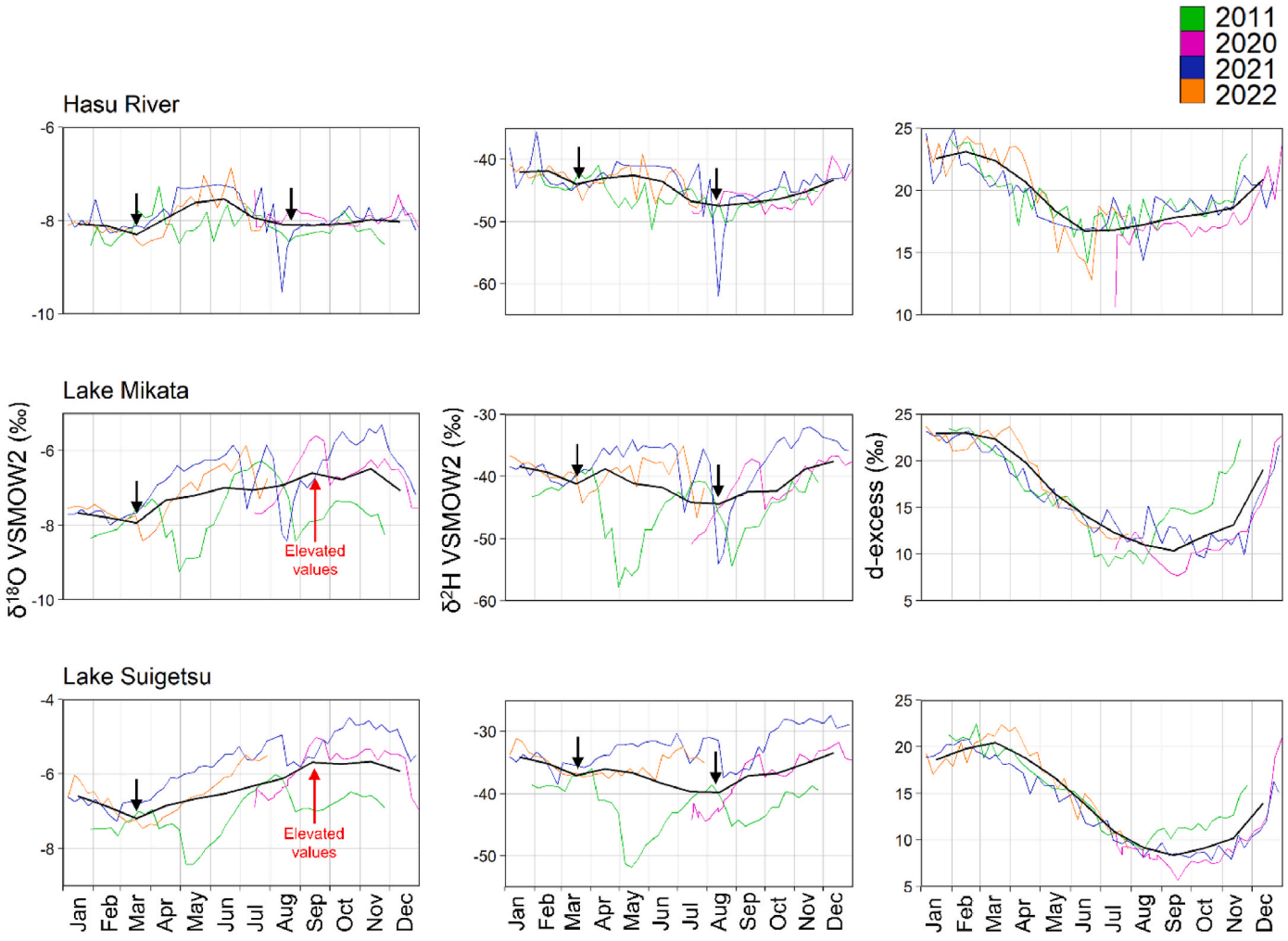

Fig. 7. Variations in δ_{river} and δ_{lake} with time. $\delta^{18}O$, $\delta^{2}H$ and d-excess values from the Hasu River, Lake Mikata and Lake Suigetsu from across the study period (colour lines). Black lines represent monthly averages of each dataset. Vertical scales are non-equivalent to best represent the shape of the data for each location. (For interpretation of the references to colour in this figure legend, the reader is referred to the Web version of this article.)

4.7. River and lake water d-excess

Despite the signal homogenisation, seasonal variations in river and lake water d-excess were very similar to precipitation d-excess, with clear differences observed across the year (Fig. 6B–D) which can be interpreted in line with the precipitation signals. This offers the most convincing evidence that $\delta_{precipitation}$ signals are detectable in δ_{lake}. However, the difference between lake water (Fig. 7) and precipitation d-excess seasonality (Fig. 4) highlights a significant modification of the precipitation signals delivered to the catchment. The seasonal extremes observed in the lakes fell during spring (high d-excess) and autumn (low d-excess; Fig. 7), in contrast to the winter and summer extremes observed in precipitation d-excess (Fig. 4). This indicates a lag of ~1–3 months between an input of precipitation and detection of this signal in lake water composition, which we attribute to the average time taken for the water to transit through the catchment. Incidentally, this interval is equivalent to the residence time of the mixolimnion, providing support for our estimation that every three months the upper ~8m of the water column is replaced with precipitation from three months previously. A comparison of Lake Suigetsu d-excess to Wakasa precipitation d-excess suggests that the transit lag was proportional to the amount of precipitation and was longer (two to three months) for the drier summer months and shorter (one to two months) during the wetter winter months. A shorter winter lag compared to summer contrasts with what might be expected for a season associated with the accumulation of snow in the catchment (which can persist on high ground for weeks at a time) and the delayed release of snowmelt to the lakes. This appears to suggest that either the snowmelt lag was negligible compared to catchment transit time, possibly because only precipitation falling on the highest ground in the catchment was delayed, or that there was still sufficient winter rainfall or rapidly melting snow to cause a response in the lake and river water within one to two months.

4.8. River and lake water $\delta^{18}O$ and $\delta^{2}H$

The river and lake water $\delta^{18}O$ and $\delta^{2}H$ values were also very similar to precipitation, exhibiting intra-seasonal variability with significant overlap (Fig. 6B–D). The Hasu River showed $\delta^{18}O$ minima in spring and late summer, a $\delta^{2}H$ minimum in late summer and slight downward inflection in $\delta^{2}H$ during spring, which were reflected in both the raw datasets and in the monthly averages (Fig. 7). Lake Mikata and Lake Suigetsu showed greater inter- and intra-annual differences than the Hasu River, but monthly averaged data from these parts of the catchment also exhibited minima in $\delta^{18}O$ in the spring and $\delta^{2}H$ in the late summer, as well as a downward inflection in $\delta^{2}H$ during the spring (Fig. 7). We relate these minima to winter (EAWM) precipitation and summer (EASM) precipitation, as detailed above in relation to precipitation $\delta^{18}O$ and $\delta^{2}H$; importantly, accounting for the aforementioned transit lag. However, unlike precipitation $\delta^{18}O$, lake $\delta^{18}O$ lacked a minimum coinciding with summer (EASM) water entering the lake; instead, there were elevated $\delta^{18}O$ values in the autumn in Lake Suigetsu (and to a lesser extent, Lake Mikata). The autumnal $\delta^{18}O$ peak (based on monthly averages) in Lake Suigetsu was approximately 3 ‰ greater than the $\delta^{18}O$ of summer precipitation. We attribute this trend to a combination of lake water mixing and saline water incursion, which brings saline water with high $\delta^{18}O$ and $\delta^{2}H$ values to the surface, causing elevated lake isotope values in autumn (discussed in Section 4.9) and a small amount of summer evaporative enrichment. We might also expect to see this trend in $\delta^{2}H$, given our proposed mechanisms, however this was not observed, likely as an artefact of a relatively small spring $\delta^{2}H$ inflection (due to high d-excess values).

Besides these elevated values of lake water $\delta^{18}O$ in summer and autumn, there is very limited evidence for an evaporation effect on the composition of lake water; a subset of summer values in each lake expressed a $\delta^{18}O$ versus $\delta^{2}H$ relationship with a reduced slope (similar to a local evaporation line), however this was restricted to the data collected in 2011 and was not present in the 2020–2022 data (Fig. 6C and D). Additionally, the $\delta^{18}O$ versus $\delta^{2}H$ slope for other seasons did not suggest evaporation effects. This highlights the potential for inter-annual variability in the influence of evaporation on lake water isotopes, but demonstrates that this effect was a secondary one and affected summer $\delta^{18}O$ and $\delta^{2}H$ alone. We posit that the enhanced evaporation in summer 2011 was due to lower relative humidity. Relative humidity data was not available from the local Mihama weather station, but the nearest data from Tsuruga, 14 km to the northeast shows that relative humidity in 2011 was on average 5 % lower than summer 2021 (Japanese Meteorological Agency, 2023). Whilst Tsuruga experiences subtly different weather conditions, it is reasonable to compare these locations on seasonal timescales.

As well as this evaporation trend, δ_{lake} in 2011 showed some discrepancies relative to the 2020–2022 interval (the data from which were broadly consistent). The data from 2011 showed a distinctive trend (a minimum in $\delta^{18}O$ and $\delta^{2}H$ in May, and an earlier increase in d-excess in the autumn). Because these trends were not observed for the Hasu River, they can be attributed to within-lake processes; however, there is no comparable precipitation isotope data available for this period in order to further interrogate this interpretation. Data from the local Mihama weather station shows intense precipitation during May 2011 (448 mm), which could have resulted in a significant direct input of low $\delta^{18}O$ and $\delta^{2}H$ water into Lake Mikata and Lake Suigetsu during this month; however, with available data this remains speculative. Overall high precipitation amounts in 2011, and hence a shorter residence time, might also explain the earlier increase in lake d-excess in autumn 2011 compared to the 2020–2022 observation period.

4.9. Vertical profiles of lake water isotopes in Lake Suigetsu

The ~quarterly depth profiling of Lake Suigetsu shows seasonal variations in the mixolimnion (above the chemocline) but compositions were consistent and homogenous in the monimolimnion year-round (Fig. 8). In the monimolimnion, temperature and salinity were consistently at ~16 °C and ~14 g kg^{-1}, respectively. Above the chemocline, the water temperature was highest in the summer and lowest in the winter. A salinity minimum was observed during the spring and maximum during the autumn, with summer and winter exhibiting intermediate values. These observations are in agreement with the findings of Kondo et al. (2000), which presented long term monitoring of changes in temperature and salinity with depth at Lake Suigetsu. Throughout the sampling period the monimolimnion waters had higher $\delta^{18}O$ and $\delta^{2}H$ values relative to the mixolimnion and showed no variation with depth between ~8 m and the lake bottom at 34 m. The d-excess values in the monimolimnion were also invariant and generally lower than the mixolimnion. In the mixolimnion, the $\delta^{18}O$, $\delta^{2}H$ and d-excess values showed smooth gradients between the chemocline and the surface, which suggests that the shape of each depth profile was driven by the difference between deepwater and surficial δ_{lake}. The d-excess depth profiles in Fig. 8 matched the seasonal fluctuations discussed above, with the highest values in spring and lowest values in autumn.

The $\delta^{18}O$, $\delta^{2}H$ and d-excess profiles did not show any correlation with temperature and hence lake water temperature is unlikely to have been a controlling factor. However, there was an increase in salinity, $\delta^{18}O$ and $\delta^{2}H$ through summer and autumn which suggests common drivers. We theorise that this trend was a result of saline water incursion and mixolimnion mixing during autumn (evidenced by Kondo et al., 2000). Summer evaporation could have enhanced this effect via the enrichment of heavier isotopes at the surface and by increasing the relative concentration of dissolved ions. There is evidence for a combination of these effects at play, because both the summer (August) and winter (November) profiles exhibited raised surface $\delta^{18}O$ and $\delta^{2}H$ values (Fig. 8); however, the evidence for evaporation trends in the surface water samples (discussed above) was limited to 2011, so we suggest that in most years evaporation was less influential than mixing. These effects

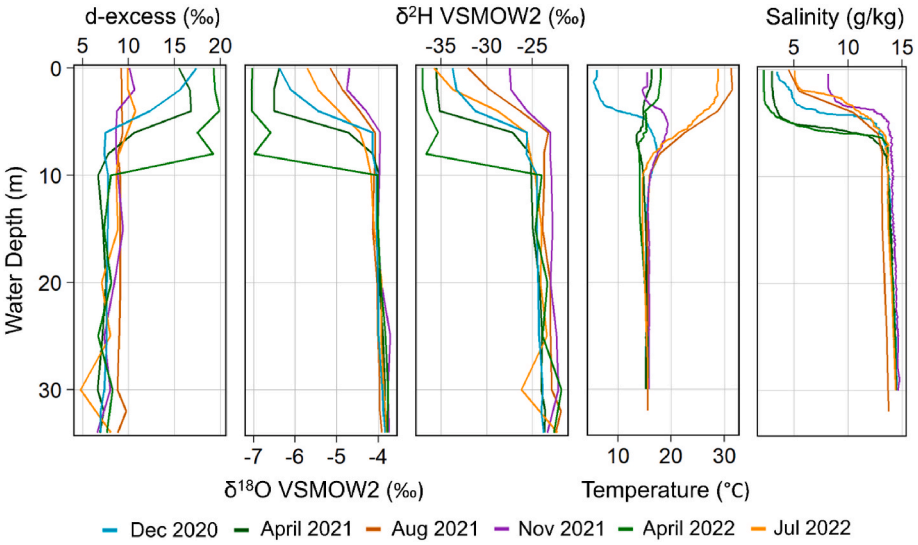

Fig. 8. Variations in Suigetsu δ_{lake} with depth. d-excess, $\delta^{18}O$, $\delta^{2}H$, temperature and salinity profiles across the study interval. Data were collected (approximately quarterly) on 22nd December 2020, 8th April 2021, 5th August 2021, 17th November 2021, 23rd April 2022 and 21st July 2022. (For interpretation of the references to colour in this figure legend, the reader is referred to the Web version of this article.)

explain the absence of a late summer $\delta^{18}O$ minimum in Lake Mikata and Lake Suigetsu (in contrast to precipitation $\delta^{18}O$) and elevated autumn values (discussed above; Fig. 7). D-excess did not appear to change significantly in autumn; possibly due to the overwhelming influence of seasonality, but most likely because the d-excess values at the surface and in the saline deep water were similar during the autumn. Hence, any amount of incursion or mixing would not result in a change in d-excess at the surface.

The combined influence of saline water incursion, mixing and evaporation did not persist through the entirety of the year; evidence from the surface water isotopes indicates that evaporation was limited to the summer, and extended monitoring by Kondo et al. (2000) suggested that mixolimnion mixing was temporally constrained to autumn. Our observations suggest that heavy winter precipitation delivered to the catchment regenerated the freshwater mixolimnion in Lake Suigetsu and effectively "reset" the effects described above, producing the minima in $\delta^{18}O$ and $\delta^{2}H$ in the surface waters (Fig. 7) and reinstating the relationship between precipitation and lake $\delta^{18}O$ and $\delta^{2}H$. However, since the surface waters of Lake Suigetsu retain some salinity year-round, the influence of saline water is never zero, merely diminished in relation to the effect of precipitation inputs. We observed an increase in $\delta^{18}O$ and $\delta^{2}H$ of the surface waters from the freshwater Hasu River to the fresh-brackish Lake Mikata and then to the brackish-saline Lake Suigetsu (Fig. 6), which was likely due to increasing quantities of Sea of Japan-derived waters (with higher isotope compositions). The composition of Lake Suigetsu showed the greatest departure from the Hasu River composition during autumn, but there was still ~1 ‰ difference in $\delta^{18}O$ during spring between the locations which can be attributed to this non-zero salinity. Lake Mikata existed between the compositions of Lake Suigetsu and the Hasu River because it is a shallower water body with no persistent saline deepwater but does experience a small degree of saline water incursion during autumn (Kondo et al., *unpublished data*) and possibly some evaporation.

5. Discussion

The key motivation of this study was to understand the major controls of δ_{river} and δ_{lake} within the Five Lakes of Mikata catchment and hence direct future interpretation of isotope-based palaeoclimate proxies from the Lake Suigetsu sediment cores. Our results show that a dominant control of Lake Suigetsu δ_{lake} (as well as Lake Mikata δ_{lake}) was the isotope composition of precipitation, and whilst there were internal catchment processes (homogenisation, a transit lag, seawater influences and evaporation) that affected the composition of river and lakes, for the most part (excluding autumn) these did not obscure the $\delta_{precipitation}$ signals, or prevent their detection in δ_{lake}. Indeed, the predominant effect of the signal homogenisation was to limit the effect of $\delta_{precipitation}$ dataset noise on δ_{lake}. In order to better understand the propagation of $\delta_{precipitation}$ signals to δ_{lake} across the span of the Suigetsu cores, it is important to consider the ways in which the current lake configuration is non-analogous to the past.

Our observations also indicate that evaporation effects were not particularly influential during the study period (with the strongest evidence limited to a single year) and were limited to the summer months. This would be expected to be the case for much of the interval covered by the Suigetsu cores, given that, aside from the Eemian, our monitoring period existed at the upper limit of temperatures experienced at the Five Lakes of Mikata for the last 150 ka. Whilst it is important to consider that evaporation is not singularly related to air temperature, but rather a range of interconnected physical processes, Lake Suigetsu receives large quantities of precipitation annually which limits the impact of evaporation on δ_{lake} (Vystavna et al., 2021). It follows that evaporation is not likely to have been a major driver of δ_{lake} across the history of Lake Suigetsu sedimentation, as long as the region was not significantly more arid in the past, but should still be considered when interpreting proxies of summer δ_{lake}.

Marine influences are also negligible from a palaeo-isotope perspective. In the modern day, saline water incursions and mixing of surface lake water with low $\delta^{18}O$ and $\delta^{2}H$ deepwater originating from the Sea of Japan had a demonstrable effect on lake $\delta^{18}O$ and $\delta^{2}H$ in the autumn months. However, the connection between Lake Suigetsu and the Sea of Japan is anthropogenic and there were no marine influences on the lakes for most of the late Pleistocene (exceptions being at ~7 ka during a highstand in the Sea of Japan, and during the Eemian global highstand) as corroborated by diatom assemblage counts of freshwater versus brackish-tolerant species (Saito-Kato et al., *unpublished data*). Aside from these intervals, we predict that δ_{lake} was not affected by seawater, either via saline water incursions or mixing. There is evidence for stratification in the past (deepwater anoxia is supported by varve preservation, and surface water oxygenation is supported by aquatic productivity); however, we would not expect to see the same stark difference in isotope compositions above and below the palaeo-chemocline

as the present-day chemocline because the deepwater and surficial waters would have had the same meteoric source. As a result, there would be no influence of the Sea of Japan to Lake Suigetsu outside of these periods and the elevated autumn $\delta^{18}O$ and $\delta^{2}H$ values that partially obscure the summer precipitation $\delta^{18}O$ minima would not be observed. Hence, in the intervals where Lake Suigetsu was a freshwater lake, we would expect $\delta_{precipitation}$ and δ_{lake} to be more closely aligned, and no offset between the Hasu River, Lake Mikata and Lake Suigetsu.

However, persistence of this stratification regime, evidenced by the preservation of varves that required basal water anoxia, suggests that the mechanistic elements of signal homogenisation (muting the seasonal precipitation signal in the surface water and homogenising the deepwater) and seasonal lags in the surface water were still active during this time, although subject to some variability. As a result, on longer timescales, palaeoclimate proxies that record deepwater conditions (e.g., isotopes of siderite ($FeCO_3$), abundant in Lake Suigetsu) would record an averaged $\delta_{precipitation}$ signal, possibly over a number of years (accounting for other fractionation processes involved in signal capture by the proxy system). Conversely, palaeoclimate proxies that record surface water conditions (e.g., diatoms and other algae) will record seasonally lagged $\delta_{precipitation}$; i.e., spring-weighted proxies will capture winter $\delta_{precipitation}$, and so forth. This relationship is of course subject to variations in the lag time (which, if lengthened, could cause greater overlap of seasonal signals) and differences in climate, which could alter the timing of delivery to the lakes. During glacial intervals, pollen reconstructed temperature for the coldest month is consistently below 0 °C, suggesting that the limited snowmelt lag in the present day would be more prominent. Additionally, the lakes were likely frozen on the surface for much of the winter. Overall, this would be expected to have stalled the movement of water through the catchment and extend the transit lag between delivery of winter (EAWM) precipitation and detection in the lake into the spring season. Under these circumstances, palaeoclimate proxies that capture the spring δ_{lake}, such as spring blooming diatoms, would capture winter (EAWM) $\delta_{precipitation}$ (arguably with even greater certainty than the present day). Proxies that capture summer δ_{lake}, such as algal biomarkers would, by contrast, capture a mix between winter, spring and summer $\delta_{precipitation}$ because these would enter the lake in quicker succession (although spring precipitation quantities are very small in comparison to winter and summer, and hence are unlikely to have a significant effect). Autumn δ_{lake}-capturing proxies, such as autumn blooming diatoms, would still predominately capture summer (EASM) $\delta_{precipitation}$ composition. Terrestrial proxies (e.g., $\delta^{18}O$ of pollen grains and $\delta^{2}H$ of long-chained n-alkanes and n-alkanoic acids) would be unaffected by changes to the transit lag as they capture soil pore water rather than lake water and would be expected to more closely reflect changing $\delta_{precipitation}$.

Having established that the dominant driver of δ_{lake} is $\delta_{precipitation}$, it is prudent to consider what could affect this quantity in the past. We anticipate that palaeo-EAM precipitation from both seasonal modes was a dominant influence on $\delta_{precipitation}$ delivered to the catchment because winter and summer are associated with large quantities of precipitation (and hence $\delta_{precipitation}$ will be weighted towards the composition of the EAWM and EASM). Additionally, whilst autumn (predominately typhoon) precipitation provides a third period of rain annually, and we observe the influence of intense precipitation events on $\delta^{18}O$ and $\delta^{2}H$ of precipitation, these signals were not detected in the lakes. For this reason, we anticipate that unless typhoon frequency was significantly greater in the past, the tendency of δ_{lake} to reflect only extended seasonal precipitation events (i.e., the EAM) will limit the influence of typhoon precipitation, even if it is recorded in $\delta_{precipitation}$. It is not unreasonable, therefore, to exclude the typhoon season influence on $\delta_{precipitation}$, and consider $\delta_{precipitation}$ at Wakasa to be most closely linked with EAM behaviour. Importantly, the influence of both EAWM and EASM components were observed at the catchment, establishing that the area is a sensitive location – even optimised, especially relative to Tokyo – for studying both components of the EAM. This is particularly useful given the skew in existing palaeoclimate reconstructions towards the summer months.

However, our findings were consistent with others from central Japan (e.g., Taniguchi et al., 2000), which note that for contemporary isotopes there is no significant difference in $\delta^{18}O$ and $\delta^{2}H$ between EAWM and EASM precipitation. As such, it is important to note that unlike Continental Asia, annually integrated $\delta^{18}O$ and $\delta^{2}H$ do not reflect the changing relative input of EAWM and EASM precipitation, because their compositions are so alike. Isotope composition averaged on multiannual timescales will not reflect the balance between these systems unless either one of EAWM or EASM changes in strength and the other remains stable, or one increases in strength and the other decreases concurrently. These changes in behaviour can be caused by different climatic regimes (such as glacial periods) or across climatic transitions. Under such conditions, the changing strength of the EAWM and EASM would be expected to impact on both the annually averaged deep δ_{lake} and the seasonally-lagged surface water δ_{lake}; the former by affecting the balance between the two seasonal modes, and the latter by affecting either EAWM or EASM $\delta_{precipitation}$. Under these circumstances, EAWM and EASM $\delta_{precipitation}$ would diverge, and hence terrestrial and surface water palaeoclimate proxy seasonality becomes extremely important for interpretation. It is therefore vital to know which composition (winter-weighted, summer-weighted or mixed) is captured by each palaeoclimate proxy before interpreting the signal, accounting also for changes to the lag time.

Our observations are restricted to the study interval, and hence provide limited contributions to the interpretation of long-term drivers of $\delta^{18}O$ and $\delta^{2}H$ associated with EAM behaviour, however this remains an important component of palaeoclimate proxy interpretation. EAM rainfall $\delta_{precipitation}$ tends to respond inversely to monsoon strength, due to a combination of preferential rainout of the heavier isotopes, enhanced by increased quantities of precipitation and increased cloud top height with a stronger monsoonal convection, which is associated with low condensation temperatures (Cai and Tian, 2016). Our results show that the amount effect does not have a strong relationship within the catchment in the modern day; however, that does not preclude a relationship to monsoon intensity; Uemura et al. (2012) noted a limited influence of local precipitation amount on $\delta^{18}O$ in Okinawa (Southern Japan), but that the precipitation amount integrated over the full transport pathway was significant. Furthermore, the Fukugaguchi stalagmite record (Itoigawa, central Japan) shows a strong relationship of $\delta^{18}O$ to EAWM precipitation amount despite modern $\delta_{precipitation}$ showing a statistically weak relationship to precipitation amount (Sone et al., 2013). Other factors which could contribute to the overall signal are changes at source: composition, temperature and relative humidity (e.g., Amekawa et al., 2021), and, in the EASM mode, the positioning of the EAM front (Kurita et al., 2015). Furthermore, the prevalence of sea ice during glacial periods, particularly in the relatively isolated Sea of Japan, might be expected to limit evaporation despite changes to EAWM strength. Hence, it is vital to consider how EAM $\delta_{precipitation}$ was controlled by the evolution of the climate of the region as a whole and how this affected $\delta_{precipitation}$ at Wakasa.

Finally, the clearest seasonal signal derived from the catchment was undoubtedly that of d-excess, and this was the only isotope parameter which demonstrated the ability to distinguish precipitation from different seasons. Not only this, but the transfer of the d-excess signal from precipitation to lake was clearer than for $\delta^{18}O$ and $\delta^{2}H$, possibly due to the amplitude of seasonal changes and the limited influence of other competing controls. However, it is much more difficult to calculate d-excess using palaeo-isotope reconstructions, because it requires the combination of temporally and spatially equivalent $\delta^{18}O$ and $\delta^{2}H$ values. If compatible palaeoclimate proxy records are produced and d-excess calculation becomes possible, this should be a consideration for future research based on the excellent seasonal distinctions observed in this variable and its potential as a powerful proxy of past monsoon dynamics.

6. Conclusions

Understanding the relationship between climate variability, the isotope composition of precipitation and the transfer of precipitation isotope signals into lake waters is essential to support the interpretation of past climates using isotope-based proxies derived from lake sediments. Using contemporary monitoring of the isotope composition of precipitation ($\delta_{precipitation}$), river water (δ_{river}) and lake water (δ_{lake}) across the Five Lakes of Mikata catchment, Japan, we assessed the factors affecting δ_{lake}, with a particular focus on Lake Suigetsu. Precipitation $\delta^{18}O$ and $\delta^{2}H$ exhibited only small seasonal differences across the year due to the similar compositions of winter (EAWM) and summer (EASM) precipitation, which act as end members with opposing trajectories. Precipitation d-excess, by contrast, clearly demarcated the different seasonal influences due to different evaporation conditions at the moisture sources of the EAWM (Sea of Japan) and EASM (Pacific Ocean domain), with a gradual shift between the two during the spring and autumn. The difference between winter and summer d-excess was enhanced by the location of the catchment. There was limited statistical evidence to support a temperature effect over precipitation $\delta^{18}O$ or $\delta^{2}H$; however, when considering the data on a seasonal basis, there was some evidence to support a local amount effect, with minima in monthly averaged $\delta^{18}O$ and $\delta^{2}H$ during the wettest (EAM) seasons of the year.

We found that δ_{lake} and $\delta_{precipitation}$ were directly related, although the spread of values of δ_{lake} was more limited due to in-catchment homogenisation. Despite this, compositional patterns were preserved, and it was still possible to detect seasonal trends in δ_{lake}, which paralleled those of $\delta_{precipitation}$ and were attributed to the same causes. A two to three-month transit lag between $\delta_{precipitation}$ and δ_{lake} was observed and the length of this lag related to the quantity of precipitation. The influence of isolated precipitation events on δ_{lake} (including typhoons) was negligible in comparison to significant extended freshwater inputs to the catchment from the East Asian Monsoon. The incursion of saline water from the Sea of Japan and autumnal mixing resulted in elevated $\delta^{18}O$ and $\delta^{2}H$ values in the lakes during late summer and autumn (obscuring the $\delta^{18}O$ minimum equated to the EASM) and caused a greater effect for Lake Suigetsu than Lake Mikata. This was possibly combined with summer evaporation effects, although evidence for the influence of evaporation varied between years. The large influx of winter precipitation to the catchment re-established the relationship between δ_{lake} and $\delta_{precipitation}$ which extended from winter to early summer. Deep water composition in Lake Suigetsu was stable and homogenous across the study period.

These results will facilitate interpretation of palaeoclimate reconstructions derived from oxygen and hydrogen isotope analysis of the Lake Suigetsu sediment cores. It is expected that $\delta_{precipitation}$ (and thus δ_{lake}) will be closely related to East Asian Summer Monsoon and East Asian Winter Monsoon $\delta_{precipitation}$ fluctuations across the ~150 ka of the late Quaternary covered by the Suigetsu cores. The seasonal patterns in δ_{lake} could be altered under different climatic regimes by large scale drivers (such as monsoon strength and balance of seasonal precipitation), along with the influence of local factors, including the transit lag. However, not all of the factors affecting δ_{lake} observed during this contemporary monitoring will be significant on longer timescales. The incursion of sea water is a consequence of anthropogenic catchment alteration and, as such, is not expected to have affected the lake water isotope hydrology prior to the last ~400 years. Evaporation is also expected to have minimal effects on down-core δ_{lake} reconstructions which are limited to the summer months. Robust interpretation is predicated on sound understanding of proxy seasonality and whether the proxy captures surficial or deepwater δ_{lake}.

Declaration of competing interest

The authors declare that they have no known competing financial interests or personal relationships that could have appeared to influence the work reported in this paper.

Data availability

Data is available at https://doi.org/10.5525/gla.researchdata.1429

Acknowledgements

The authors would like to thank T. Tanabe for their contribution to collecting the water samples in 2011–2012, K. Ichiyanagi and M. Tanoue for permission to use their precipitation isotope data from Tokyo and R. Kondo for access to contemporary salinity data for the Five Lakes of Mikata. All other isotope analysis was conducted by C. Arrowsmith; J. Lacey contributed to the writing of the methodology section; and M. Ankor designed and built the rainwater sampler. Water quality data for the water column of Suigetsu Lake were provided by Dr Yasushi Miyamoto. This research was financially supported by an Australian Research Council Discovery Project [grant number DP200101768], a JSPS KAKENHI Grant [grant number 19K20442] and C.L.Rex was supported by the NERC IAPETUS2 Doctoral Training Partnership. The authors declare no conflicts of interest.

Appendix A. Supplementary data

Supplementary data to this article can be found online at https://doi.org/10.1016/j.qsa.2023.100145.

References

Amekawa, S., Kashiwagi, K., Hori, M., Sone, T., Kato, H., Okumura, T., Yu, T.L., Shen, C. C., Kano, A., 2021. Stalagmite evidence for East Asian winter monsoon variability and 18O-depleted surface water in the Japan Sea during the last glacial period. Prog. Earth Planet. Sci. 8 (1) https://doi.org/10.1186/s40645-021-00409-8.

Araguás-Araguás, L., Froehlich, K., Rozanski, K., 1998. Stable isotope composition of precipitation over southeast Asia. J. Geophys. Res. Atmos. 103 (D22), 28721–28742. https://doi.org/10.1029/98JD02582.

Bershaw, J., 2018. Controls on deuterium excess across Asia. Geosciences 8 (7), 257. https://doi.org/10.3390/geosciences8070257.

Bronk Ramsey, C., Staff, R.A., Bryant, C.L., Brock, F., Kitagawa, H., Van Der Plicht, J., Schlolaut, G., Marshall, M.H., Brauer, A., Lamb, H.F., Payne, R.L., Tarasov, P.E., Haraguchi, T., Gotanda, K., Yonenobu, H., Yokoyama, Y., Tada, R., Nakagawa, T., 2012. A complete terrestrial radiocarbon record for 11.2 to 52.8 kyr B.P. Science 338 (6105), 370–374. https://doi.org/10.1126/science.1226660.

Bronk Ramsey, C., Heaton, T.J., Schlolaut, G., Staff, R.A., Bryant, C.L., Brauer, A., Lamb, H.F., Marshall, M.H., Nakagawa, T., 2020. Reanalysis of the atmospheric radiocarbon calibration record from Lake Suigetsu, Japan. Radiocarbon 62 (4), 989–999. https://doi.org/10.1017/RDC.2020.18.

Esri, 2022a. "World Dark Grey base" [basemap] 1:10,000,000 (panel A), 1:400,000 (panel B), 1:67,946 (panel C). https://www.arcgis.com/home/item.html?id=a284a9b99b3446a3910d4144a50990f6. (Accessed 12 September 2022).

Esri, 2022b. "World Hillshade" [basemap] 1:10,000,000 (panel A), 1:400,000 (panel B), 1:67,946 (panel C). https://www.arcgis.com/home/item.html?id=1b243539f4514b6ba35e7d995890db1d. (Accessed 12 September 2022).

Fudeyasu, H., Ichiyanagi, K., Sugimoto, A., Yoshimura, K., Ueta, A., Yamanaka, M.D., Ozawa, K., 2008. Isotope ratios of precipitation and water vapor observed in Typhoon Shanshan. J. Geophys. Res. Atmos. 113 https://doi.org/10.1029/2007JD009313 article D12113.

Gallagher, S.J., Sagawa, T., Henderson, A.C.G., Saavedra-Pellitero, M., De Vleeschouwer, D., Black, H., Itaki, T., Toucanne, S., Bassetti, M.A., Clemens, S., Anderson, W., Alvarez-Zarikian, C., Tada, R., 2018. East asian monsoon history and paleoceanography of the Japan sea over the last 460,000 years. Paleoceanogr. Paleoclimatol. 33 (7), 683–702. https://doi.org/10.1029/2018PA003331.

Gibson, J.J., Birks, S.J., Yi, Y., 2016. Stable isotope mass balance of lakes: a contemporary perspective. Quat. Sci. Rev. 131, 316–328. https://doi.org/10.1016/j.quascirev.2015.04.013.

Gonfiantini, R., 1986. Environmental isotopes in lake studies. In: Fritz, P., Fontes, J.C. (Eds.), Handbook of Environmental Isotope Geochemistry Volume Two, the Terrestrial Environment. Elsevier, B. Netherlands, pp. 113–168. https://doi.org/10.1016/B978-0-444-42225-5.50008-5.

Hasegawa, H., Akata, N., Kawabata, H., Sato, T., Chikuchi, Y., Hisamatsu, S., 2014. Characteristics of hydrogen and oxygen stable isotope ratios in precipitation collected in a snowfall region, Aomori Prefecture, Japan. Geochem. J. 48 (1), 9–18. https://doi.org/10.2343/geochemj.2.0279.

Ichiyanagi, K., Tanoue, M., and on behalf of the Isotope Mapping Working Group of the Japanese Society of Hydrological Science (IMWG/JAHS), 2016. Spatial analysis of annual mean stable isotopes in precipitation across Japan based on an intensive

observation period throughout 2013. Isotopes Environ. Health Stud. 52 (4–5), 353–362. https://doi.org/10.1080/10256016.2015.1132215.
Ichiyanagi, K., Tanoue, M., 2016. Stable isotopes in precipitation across Japan during an intensive observation period throughout 2013. J. Jpn. Assoc. Hydrol. Sci. 46 (2), 123–138. https://doi.org/10.4145/jahs.46.123.
Jackisch, D., Yeo, B.X., Switzer, A.D., He, S., Cantarero, D.L.M., Siringan, F.P., Goodkin, N.F., 2022. Precipitation stable isotopic signatures of tropical cyclones in Metropolitan Manila, Philippines, show significant negative isotopic excursions. Nat. Hazards Earth Syst. Sci. 22 (1), 213–226. https://doi.org/10.5194/nhess-22-213-2022.
Japanese Meteorological Agency, 2022. Mihama (Fukui Prefecture) JMA Weather Station Data, Electronic Dataset, Japanese Meteorological Agency viewed 10/02/2022. https://www.data.jma.go.jp/risk/obsdl/index.php.
Japanese Meteorological Agency, 2023. Tsuruga (Fukui Prefecture) JMA Weather Station Data, Electronic Dataset, Japanese Meteorological Agency viewed 23/06/2023. https://www.data.jma.go.jp/risk/obsdl/index.php.
Jun-Mei, L., Jian-Hua, J., Shi-Yan, T., 2013. Re-discussion on East Asian Meiyu rainy season. Atmos. Oceanic Sci. Lett. 6, 279–283. https://doi.org/10.3878/j.issn.1674-2834.13.0024.
Kondo, R., Butani, J., 2007. Comparison of the diversity of sulfate-reducing bacterial communities in the water column and the surface sediments of a Japanese meromictic lake. Limnology 8, 131–141. https://doi.org/10.1007/s10201-007-0201-9.
Kondo, R., Kasashima, N., Matsuda, H., Hata, Y., 2000. Determination of thiosulfate in a meromictic lake. Fish. Sci. 66 (6), 1076–1081. https://doi.org/10.1046/j.1444-2906.2000.00171.x.
Kondo, R., Kodera, M., Mori, Y., Okamura, T., Yoshikawa, S., Ohki, K., 2014. Spatiotemporal distribution of bacteriochlorophylls in the meromictic Lake Suigetsu, Japan. Limnology 15, 77–83. https://doi.org/10.1007/s10201-013-0415-y.
Kurita, N., Fujiyoshi, Y., Nakayama, T., Matsumi, Y., Kitagawa, H., 2015. East Asian Monsoon controls on the inter-annual variability in precipitation isotope ratio in Japan. Clim. Past 11, 339–353. https://doi.org/10.5194/cp-11-339-2015.
Lawrence, R.J., Gedzelman, D.S., 1996. Low stable isotope ratios of tropical cyclone rains. Geophys. Res. Lett. 23 (5), 527–530. https://doi.org/10.1029/96GL00425.
Li, C., Kano, N., Ueno, Y., Hanabusa, M., Jiao, Y., Imaizumi, H., Watanabe, N., 2010. Characteristics of oxygen stable isotopic ratio in precipitations in Niigata Prefecture, Japan. Radioisotopes 59 (2), 93–102. https://doi.org/10.3769/radioisotopes.59.93.
Masuzawa, T., Kitano, Y., 1982. Diagenetic deposition of manganese in sediment of a historically meromictic lake, Lake Suigetsu, Japan. J. Oceanogr. Soc. Jpn. 38, 73–80. https://doi.org/10.1007/BF02110293.
Matsuyama, M., 1973. Changes in the Limnological features of a meromictic Lake Suigetsu during the years, 1926-1967. J. Oceanogr. 29, 131–139. https://doi.org/10.1007/BF02109088.
Matsuyama, M., 1974. Vertical distributions of some chemical substances in surface sediments of a meromictic Lake Suigetsu. J. Oceanogr. Soc. Jpn. 30, 209–215. https://doi.org/10.1007/BF02111046.
McLean, D., Albert, P.G., Nakagawa, T., Staff, R.A., Suzuki, T., Smith, V.C., 2016. Identification of the Changbaishan 'Millennium' (B-Tm) eruption deposit in the Lake Suigetsu (SG06) sedimentary archive, Japan: synchronisation of hemispheric-wide palaeoclimate archives. Quat. Sci. Rev. 150, 301–307. https://doi.org/10.1016/j.quascirev.2016.08.022.
Nakagawa, T., Gotanda, K., Haraguchi, T., Danhara, T., Yonenobu, H., Brauer, A., Yokoyama, Y., Tada, R., Takemura, K., Staff, R.A., Payne, R.L., Bronk Ramsey, C., Bryant, C.L., Brock, F., Schlolaut, G., Marshall, M.H., Tarasov, P.E., Lamb, H.F., 2012. SG06, a fully continuous and varved sediment core from Lake Suigetsu, Japan: stratigraphy and potential for improving the radiocarbon calibration model and understanding of late Quaternary climate changes. Quat. Sci. Rev. 36, 164–176. https://doi.org/10.1016/j.quascirev.2010.12.013.
Nakagawa, T., Tarasov, P., Staff, R., Bronk Ramsey, C., Marshall, M., Schlolaut, G., Bryant, C., Brauer, A., Lamb, H., Haraguchi, T., Gotanda, K., Kitaba, I., Kitagawa, H., van der Plicht, J., Yonenobu, H., Omori, T., Yokoyama, Y., Tada, R., Yasuda, Y., 2021. The spatio-temporal structure of the Lateglacial to early Holocene transition reconstructed from the pollen record of Lake Suigetsu and its precise correlation with other key global archives: implications for palaeoclimatology and archaeology. Global Planet. Change 202, 103493. https://doi.org/10.1016/j.gloplacha.2021.103493.
Rolph, G., Stein, A., Stunder, B., 2017. Real-time environmental applications and display sYstem: READY. Environ. Model. Software 95, 210–228. https://doi.org/10.1016/j.envsoft.2017.06.025.
Russell, J.M., Johnson, T.C., 2006. The water balance and stable isotope hydrology of Lake Edward, Uganda-Congo. J. Great Lake. Res. 32 (1), 77–90. https://doi.org/10.3394/0380-1330(2006)32[77:TWBASI]2.0.CO;2.
Schlolaut, G., Marshall, M.H., Brauer, A., Nakagawa, T., Lamb, H.F., Staff, R.A., Bronk Ramsey, C., Bryant, C.L., Brock, F., Kossler, A., Tarasov, P.E., Yokoyama, Y., Tada, R., Haraguchi, T., 2012. An automated method for varve interpolation and its application to the Late Glacial chronology from Lake Suigetsu, Japan. Quat. Geochronol. 13, 52–69. https://doi.org/10.1016/j.quageo.2012.07.005.
Schlolaut, G., Brauer, A., Nakagawa, T., Lamb, H.F., Tyler, J.J., Staff, R.A., Marshall, M.H., Bronk Ramsey, C., Bryant, C.L., Tarasov, P.E., 2017. Evidence for a bi-partition of the younger dryas Stadial in East Asia associated with inversed climate characteristics compared to Europe. Sci. Rep. 7, 44983 https://doi.org/10.1038/srep44983.
Schlolaut, G., Staff, R.A., Brauer, A., Lamb, H.F., Marshall, M.H., Bronk Ramsey, C., Nakagawa, T., 2018. An extended and revised Lake Suigetsu varve chronology from ~50 to ~10 ka BP based on detailed sediment micro-facies analyses. Quat. Sci. Rev. 200, 351–366. https://doi.org/10.1016/j.quascirev.2018.09.021.
Seal, R.R., Shanks, W.C., 1998. Oxygen and hydrogen isotope systematics of Lake Baikal, Siberia: implications for paleoclimate studies. Limnol. Oceanogr. 43 (6), 1251–1261. https://doi.org/10.4319/lo.1998.43.6.1251.
Shigematsu, T., Tabushi, M., Nishikawa, Y., Muroga, T., Matsunaga, Y., 1961. Geochemical study on lakes Mikata. Bull. Inst. Chem. Res. Kyoto Univ. 39 (1), 43–56.
Smith, V.C., Mark, D.F., Staff, R.A., Blockley, S.P., Bronk Ramsey, C., Bryant, C.L., Nakagawa, T., Han, K.K., Weh, A., Takemura, K., Danhara, T., 2011. Toward establishing precise $^{40}Ar/^{39}Ar$ chronologies for Late Pleistocene palaeoclimate archives: an example from the Lake Suigetsu (Japan) sedimentary record. Quat. Sci. Rev. 30 (21–22), 2845–2850. https://doi.org/10.1016/j.quascirev.2011.06.020.
Sone, T., Kano, A., Okumura, T., Kashiwagi, K., Hori, M., Jiang, X., Shen, C.C., 2013. Holocene stalagmite oxygen isotopic record from the Japan Sea side of the Japanese Islands, as a new proxy of the East Asian winter monsoon. Quat. Sci. Rev. 75, 150–160. https://doi.org/10.1016/j.quascirev.2013.06.019.
Staff, R.A., Ramsey, C.B., Bryant, C.L., Brock, F., Payne, R.L., Schlolaut, G., Marshall, M.H., Brauer, A., Lamb, H.F., Tarasov, P.E., Yokoyama, Y., Haraguchi, T., Gotanda, K., Yonenobu, H., Nakagawa, T., 2011. New ^{14}C determinations from Lake Suigetsu, Japan: 12,000 to 0 cal BP. Radiocarbon 53 (3), 511–528. https://doi.org/10.1017/S0033822200034627.
Stein, A.F., Draxler, R.R., Rolph, G.D., Stunder, B.J.B., Cohen, M.D., Ngan, F., 2015. NOAA's HYSPLIT atmospheric transport and dispersion modeling system. Bull. Am. Meteorol. Soc. 96 (12), 2059–2077. https://doi.org/10.1175/BAMS-D-14-00110.1.
Taniguchi, M., Nakayama, T., Tase, N., Shimada, J., 2000. Stable isotope studies of precipitation and river water in the Lake Biwa basin, Japan. Hydrol. Process. 14 (3), 539–556. https://doi.org/10.1002/(SICI)1099-1085(20000228)14:3<539::AID-HYP953>3.0.CO;2-L.
Uemura, R., Yonezawa, N., Yoshimura, K., Asami, R., Kadena, H., Yamada, K., Yoshida, N., 2012. Factors controlling isotopic composition of precipitation on Okinawa Island, Japan: implications for paleoclimate reconstruction in the East Asian Monsoon region. J. Hydrol. 475, 314–322. https://doi.org/10.1016/j.jhydrol.2012.10.014.
Vystavna, Y., Harjung, A., Monteiro, L.R., Matiatos, I., Wassenaar, L.I., 2021. Stable isotopes in global lakes integrate catchment and climatic controls on evaporation. Nat. Commun. 12, 1–7. https://doi.org/10.1038/s41467-021-27569-x.
Walker, M.J., Johnsen, S.J., Rasmussen, S.O., Popp, T., Steffensen, J.-P., Gibbard, P., Hoek, W.Z., Lowe, J., Andrews, J., Bjo, S., Cwynar, L.C., Hughen, K.A., Kershaw, P., Kromer, B., Litt, T., Lowe, D.J., Nakagawa, T., Newnham, R., Schwander, J., Rck, B., 2009. Formal definition and dating of the GSSP (Global Stratotype Section and Point) for the base of the Holocene using the Greenland NGRIP ice core, and selected auxiliary records. J. Quat. Sci. 24 (1), 3–17. https://doi.org/10.1002/jqs.1227.
Wassenaar, L.I., Athanasopoulos, P., Hendry, M.J., 2011. Isotope hydrology of precipitation, surface and ground waters in the Okanagan Valley, British Columbia, Canada. J. Hydrol. 411 (1–2), 37–48. https://doi.org/10.1016/j.jhydrol.2011.09.032.
Xia, C., Liu, G., Hu, Y., Meng, Y., 2018. Precipitation stable isotope variability in tropical monsoon climatic zone of Asia. IOP Conf. Ser. Mater. Sci. Eng. 392 (4) https://doi.org/10.1088/1757-899X/392/4/042028.
Xia, Z., Welker, J.M., Winnick, M.J., 2022. The seasonality of deuterium excess in non-polar precipitation. Global Biogeochem. Cycles 36 (10), e2021GB007245. https://doi.org/10.1029/2021GB007245.
Xu, H., Goldsmith, Y., Lan, J., Tan, L., Wang, X., Zhou, X., Cheng, J., Lang, Y., Liu, C., 2020. Juxtaposition of western Pacific subtropical high on asian summer monsoon shapes subtropical East Asian precipitation. Geophys. Res. Lett. 47 (3), e2019GL084705 https://doi.org/10.1029/2019GL084705.